



HAL
open science

Topology optimization of frequency dependent viscoelastic structures via a level-set method

G Delgado, M Hamdaoui

► **To cite this version:**

G Delgado, M Hamdaoui. Topology optimization of frequency dependent viscoelastic structures via a level-set method. 2017. hal-01651913v1

HAL Id: hal-01651913

<https://hal.science/hal-01651913v1>

Preprint submitted on 29 Nov 2017 (v1), last revised 3 Dec 2018 (v3)

HAL is a multi-disciplinary open access archive for the deposit and dissemination of scientific research documents, whether they are published or not. The documents may come from teaching and research institutions in France or abroad, or from public or private research centers.

L'archive ouverte pluridisciplinaire **HAL**, est destinée au dépôt et à la diffusion de documents scientifiques de niveau recherche, publiés ou non, émanant des établissements d'enseignement et de recherche français ou étrangers, des laboratoires publics ou privés.

Topology optimization of frequency dependent viscoelastic structures via a level-set method

G. Delgado (IRT SystemX, Paris-Saclay, France)
M. Hamdaoui (LEM3, Université de Lorraine, France)

November 28, 2017

Abstract

Viscoelastic materials follow a liquid-like elastic behavior whose characteristics depend on the excitation frequency. Nowadays, these type of materials represent a high interest for vibration damping treatments in the automotive and aeronautic industries, for instance. This work is devoted to the application of the level-set method for topology optimization of viscoelastic structures. We look for the best distribution of viscoelastic material within a reference domain for the design of purely viscoelastic 3D damping structures and 2D viscoelastic damping treatments. In both cases one desires to maximize the structure capacity to dissipate energy measured here by the modal loss factor of the first vibration mode.

Keywords: Topology optimization, Level-set method, Viscoelastic dumping, Non-linear eigenvalue problem.

1 Introduction

Viscoelastic damping material behavior occurs in a wide variety of materials and can be characterized by liquid-like elastic behavior. Materials that experience viscoelastic behavior include acrylics, rubber, and adhesives. The characteristics of viscoelastic materials depend on temperature and frequency. Viscoelastic materials have the property of absorbing vibrational energy which makes them very interesting for structural damping applications. The vibrations can be caused by noises that radiate from a certain source as sound or structure oscillations coming from dynamical wind loadings or earthquakes. Viscoelastic dampers can be designed as 3D parts of a structure but also as damping treatments which consist of any material (or combination of materials) applied to a component to increase its ability to dissipate mechanical energy. They are most often useful when applied to a structure that is forced to vibrate at or near its natural (resonant) frequencies, is acted on by forces made up of many frequency components, is subjected to impacts or other transient forces, or transmits vibration to noise-radiating surfaces. The energy dissipation of a viscoelastic structure is typically quantified in terms of a loss factor, a dimensionless quantity that can be measured or predicted from a modal analysis or frequency response curves. Two categories of treatments for structural damping exist, the unconstrained layer damping (UCLD), where the material is simply attached with a strong bonding agent to the surface of a structure, and Constrained-layer damping (CLD) where the material is sandwiched between a base layer and a third constraining layer. The CLD treatment provides considerably more damping effect than the free viscoelastic treatment in spite of its relative complexity. Energy dissipation is achieved in this case by shearing a viscoelastic polymer between a base structure and a constraining layer. Both types of damping structure are depicted in Figures 1 and 2.

Topology optimization is essentially an iterative numerical process that seeks to find the best material layout (within a prescribed design domain) according to a given objective function and a set of design constraints, providing valuable help in problems where mechanical intuition is limited. Topology optimization of viscoelastic UCLD and CLD has been performed by many authors in the literature using different methods. Zheng *et al.* [18] used the Solid Isotropic Material with Penalization (SIMP) method with the Method of Moving Asymptote (MMA) to perform topology optimization of a CLD cantilever plate treated with DYAD606 where a sum of modal loss factors is maximized. Kim [16] applied SIMP and Evolutionary Structural Optimization (ESO) methods to design damping treatments for unconstrained-layer plate and shell structures. Zheng *et al.* [27] used the same methodology to perform topology optimization of CLD with partial coverage, showing interesting performances of the optimized

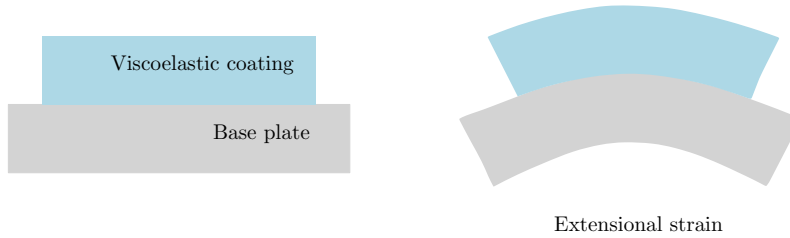


Figure 1: Unconstrained-layer damping treatment.

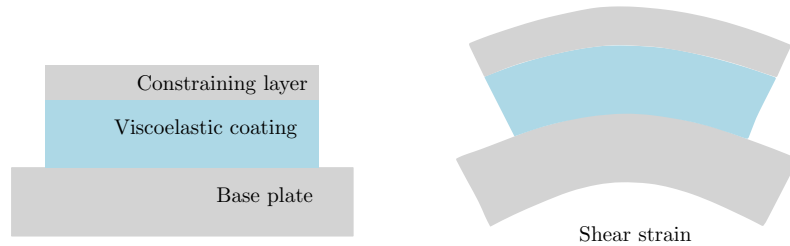


Figure 2: Constrained-layer damping treatment.

structure in terms of damping and mass savings. Kim *et al.* [17] used the rational approximation for material properties (RAMP) with the optimality criteria method (OC) to perform topology optimization of UCLD shell structures to maximize modal loss factors. El-Sabbagh *et al.* [7] used the method presented in [5] along with the MMA method to perform optimization of periodic and non-periodic plates. Zhanpeng *et al.* [8] used evolutionary structural optimization (ESO) to minimize viscoelastic CLD plate response. James *et al.* [12] used a time dependent adjoint method along with the MMA method to perform topology optimization of viscoelastically damped beams for minimum mass under time dependent loadings. Yun *et al.* [26] performed multimaterial topology optimization to maximize energy dissipation of viscoelastically damped structures subjected to unsteady loads using SIMP and MMA. Ansari *et al.* [4] used a level set method to perform topology optimization of viscoelastic UCLD plate whereas van der Kolk *et al.* [23] used a parametrized level set based method for multi-material topology optimization of beams.

The present work addresses the structural optimization of fully viscoelastic structures and UCLD treatments by means of the level-set method for topology optimization. For that purpose we rely on the level-set approach for multi-phase optimization detailed by Allaire *et al.* [1]. First introduced by Osher and Sethian [19], the level-set method has the advantage of tracking the interfaces on a fixed mesh, easily managing topological changes without remeshing. Combined to the Hadamard method of shape differentiation in the framework of structural optimization [3, 24], the level-set approach is an efficient shape and topology optimization algorithm, which gives a better description and control of the geometrical properties of the interface, avoiding typical drawbacks such as intermediate density penalization and possible spurious physical behavior during the optimization process. Moreover, as remarked by Allaire *et al.* [2], the level-set method is especially well suited for vibration problems involving eigenfrequency optimization, since small holes or material islands cannot suddenly appear or disappear between two successive iterations as they do with the homogenization or SIMP methods, thus avoiding spurious modes in low density regions.

This article is organized as follows. Section 2 is devoted to the mathematical description of viscoelastic materials and the vibration problem arising for purely viscoelastic structures and unconstrained layer damping plates. Section 3 is concerned with the study of the non-linear eigenvalue problem that stems from the aforementioned models. We provide a theoretical result characterizing the eigenvalues of such problems for a general class of viscoelastic materials. Section 4 details the sensitivity analysis of the first eigenfrequency of the structure with respect to the viscoelastic shape, and Section 5 recalls the use of the level-set method in the framework of topology optimization. Finally Section 6 outlines the numerical solution of the underlying non-linear eigenvalue problem and illustrates it with two concrete applications.

2 Setting of the problem

Let \hat{f} be the Laplace transform of a real valued function $f(t)$ defined as

$$\hat{f} = \int_0^{\infty} e^{-\mu t} f(t) dt, \quad \mu \in \mathbb{C}. \quad (1)$$

Also let $\omega \in \mathbb{C}$ be the complex pulsation describing an oscillating damped signal with angular frequency $\text{Re}(\omega)$ and relaxation time $\text{Im}(\omega)^{-1}$. Set $\mu = i\omega$ in (1).

For viscoelastic materials, a linear elastic constitutive relationship using Hooke's law is not an accurate model and a complex modulus is extensively used to describe the dynamic characteristics of viscoelastic materials [13]. The stress-strain relationship of a linear viscoelastic damping material subjected to steady-state oscillatory conditions thus reads:

$$\hat{\sigma}(\omega) = A(\omega)\hat{\epsilon}(\omega), \quad (2)$$

where ω is the complex pulsation, A is the complex (or dynamic) elastic tensor and $\hat{\sigma}$ and $\hat{\epsilon}$ are the Laplace transforms of stress and the strain, respectively. This relation stems from the Laplace transform of the stress history given by

$$\sigma(t) = \int_0^t Y(t-\tau) \frac{d\epsilon(\tau)}{d\tau} d\tau, \quad (3)$$

with Y the relaxation function (or relaxation modulus) and

$$A = i\omega\hat{Y}(\omega).$$

The relaxation function Y accounts for the material stress behavior in a relaxation test (gradual disappearance of stresses from a viscoelastic medium after it has been deformed) and the Boltzmann superposition principle (the state of stress or deformation of a viscoelastic body is a function of all the stresses applied to the material) [9].

Let (Ω, \mathcal{O}) be two bounded open sets with $\Omega \subset \mathcal{O} \subset \mathbb{R}^d$ ($d \in \{2, 3\}$).

- If $d = 3$, we will say that Ω is occupied by a viscoelastic material with complex elastic tensor A and density $\rho > 0$ within a reference (or working) domain \mathcal{O} . The boundary of Ω is made of two disjoint parts

$$\partial\Omega = \Gamma_N \cup \Gamma_D,$$

with Dirichlet boundary conditions on Γ_D and Neumann boundary conditions on Γ_N .

- If $d = 2$, \mathcal{O} will be the reference configuration for a plate in the xy -plane and Ω the surface occupied by the viscoelastic coating. By abuse of notation, we split the boundary of \mathcal{O} ($\partial\mathcal{O} = \Gamma_N \cup \Gamma_D$) instead of Ω since no boundary conditions are imposed on $\partial\Omega$.

2.1 3D viscoelastic structure

We denote by $\omega \in \mathbb{C}$ the complex pulsation and by $\hat{u} \in H^1(\Omega; \mathbb{C})^3$ the associated mode, i.e. the corresponding displacement field in Ω . For the sake of simplicity, we will generally write u unless we want to explicitly emphasize the Laplace transform. The pair (ω, u) is a solution of the non-linear eigenvalue problem

$$\begin{cases} -\text{div}(A(\omega)e(u)) = \omega^2 \rho u & \text{in } \Omega, \\ u = 0 & \text{on } \Gamma_D, \\ A(\omega)e(u) \cdot n = 0 & \text{on } \Gamma_N. \end{cases} \quad (4)$$

The state equation in (4) stems from applying the constitutive equation (2) and the Laplace transform to the evolution (wave) equation of linear elasticity

$$\rho u_{tt} - \text{div}(\sigma) = 0 \text{ in } \Omega. \quad (5)$$

We remark that the eigenvalue problem (4) is non-linear since the complex elastic (or stiffness) tensor A also depends on ω .

2.2 Composite sandwich structure

For modeling vibration damping treatments we use a plate model approximation of (4). Consider the small transverse vibration of a uniform plate with thickness $h(x)$, density $\rho(x)$ and reference configuration for the plate \mathcal{O} with $d = 2$. The transverse displacement of x at time t is denoted as $w(x, t)$ but for the sake of simplicity, we rather denote as w (instead of \hat{w}) the vertical displacement mode associated with the complex pulsation $\omega \in \mathbb{C}$.

2.2.1 Unconstrained-layer damping (UCLD) modeling

UCLD is one of the simplest forms of material application. The material is simply attached with a strong bonding agent to the surface of a structure. Energy is dissipated as a result of extension and compression of the damping material under flexural stress from the base structure. From now on, for every general quantity ξ defined either on the viscoelastic coating, the base plate or the global composite (viscoelastic coating plus base plate), we will use the notations ξ_c, ξ_p, ξ_g respectively. The following assumptions are made:

- Transverse shear and rotatory and in-plane inertia effects in both the plate and the coating are negligible for the lower modes of vibration,
- There are no applied in-plane loads,
- Displacements are small and changes in thickness are negligible,
- The viscoelastic coating is applied to only one side of the plate
- The plate and the coating are homogeneous and isotropic, and subjected to a state of plane stress,
- Displacements are continuous across the interface between the plate and the coating,
- Poisson's ratio of the coating is a real constant and the coating is incompressible ($\nu = 0.5$).

Under these assumptions, classical Kirchhoff-Love plate theory can be used. Let $w \in H^2(\mathcal{O}; \mathbb{C})$. Then the pair (ω, w) is solution of the non-linear eigenvalue problem

$$\begin{cases} -\nabla^2 : (D(\omega)\nabla^2 w) = \omega^2 \rho w & \text{in } \mathcal{O}, \\ w = 0, \nabla w = 0 & \text{on } \Gamma_D, \\ (D(\omega)\nabla^2 w)_{nn} = 0 & \text{on } \Gamma_N. \end{cases} \quad (6)$$

The aforementioned state equation follows from the virtual work principle applied to the total energy of the plate (bending strain energy plus kinetic energy) and the Laplace transform. The function $\rho(x)$ is piece-wise constant and corresponds to the surface density

$$\rho(x) = \begin{cases} \rho_p := \rho_p^V h_p & \text{if } x \in \mathcal{O} \setminus \Omega, \\ \rho_g := (\rho_p^V h_p + \rho_c^V h_c) & \text{if } x \in \Omega, \end{cases}$$

with ρ_p^V, ρ_c^V and h_p, h_c the volumetric densities and thickness of the plate and the viscoelastic coating, respectively. The equivalent bending stiffness tensor D for an isotropic base and coating material reads [20]

$$D(\omega, x) = \begin{cases} D_p := \frac{h_p^3}{12} A_p & \text{if } x \in \mathcal{O} \setminus \Omega, \\ D_g := \left(\frac{h_p^3}{12} + h_p h_n^2 \right) A_p + \left(\frac{h_c^3}{12} + h_c (h_{pc} - h_n)^2 \right) A_c(\omega) & \text{if } x \in \Omega, \end{cases} \quad (7)$$

where the tensors $A_p, A_c(\omega)$ stand for the extensional stiffness tensors of the base and viscoelastic materials respectively (we remark that only the coating material depends on ω),

$$A_l = \frac{E_l}{(1 - \nu_l^2)} \begin{pmatrix} 1 & \nu_l & 0 \\ \nu_l & 1 & 0 \\ 0 & 0 & 0.5(1 - \nu_l) \end{pmatrix}, \quad \text{with the index } l = p, c,$$

h_{pc} represents the distance between the neutral planes of the base plate and the viscoelastic layer material and h_n (see Figure 3) represents the distance between the composite neutral axis and the base plate neutral plane which can be approximated as

$$h_n = \frac{E_c h_c h_{pc}}{E_p h_p + E_c h_c}. \quad (8)$$

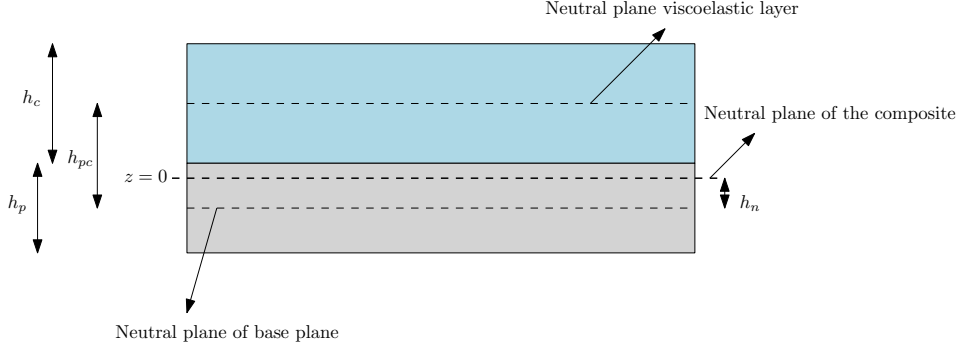


Figure 3: Neutral plane of the composite plate.

The structure of the tensor D ensues from the integration of the laminate through the thickness moment resultants meanwhile the correction terms h_n, h_{pe} arise when $h_p \neq h_c$ in order to compensate the shift of the neutral fiber of the laminate, i.e. the place in the plate where the thickness-averaged stresses vanish.

2.3 Objective function

For the sake of clarity, we detail the objective function only within the damping optimization context exposed in Section 2.1. The same notions however remain valid for viscoelastic damping treatments. Supposing that (4) admits a countable infinite family of solutions $(\omega_k, u_k)_{k \geq 1}$ in $\mathbb{C} \times H^1(\Omega; \mathbb{C})^3$ (see more details in the next section), with the eigenfunctions or modes normalized by imposing that $\int_{\Omega} \rho |u_k|^2 dx = 1$, the objective function $\eta(\Omega)$ to be maximized is the modal loss factor of the structure for its first eigenvalue:

$$\eta(\Omega) := \frac{\text{Im}(\omega_1^2)}{\text{Re}(\omega_1^2)} = \frac{\text{Im} \left(\int_{\Omega} A e(u) : e(\bar{u}) dx \right)}{\text{Re} \left(\int_{\Omega} A e(u) : e(\bar{u}) dx \right)}, \quad (9)$$

where \bar{u} is the complex conjugate of u and η represents the ratio between dissipated and stored energy, in other words, the structure capacity to dissipate energy. We recall that we focus only on the loss factor associated with the first resonant frequency within this work. The concept of modal loss factor, which fulfills the relation

$$\omega_1^2 = \text{Re}(\omega_1^2)(1 + i\eta),$$

derives from the notion of material loss factors of a viscoelastic material, which allows to express for instance the complex Young and shear moduli $E(\omega), G(\omega)$ via the Young and shear moduli factors η_E, η_G as:

$$E = \text{Re}(E)(1 + i\eta_E) \quad \text{and} \quad G = \text{Re}(G)(1 + i\eta_G). \quad (10)$$

Since the eigenvalues of (4) cannot be naturally ordered in \mathbb{C} , ω_1 will be defined as the closest eigenvalue of (4) to ω_1^ℓ (in the sens of modulus $|\omega_1 - \omega_1^\ell|$), where $(\omega_k^\ell, u_k^\ell)_{k \geq 1}$ in $\mathbb{R} \times H^1(\Omega; \mathbb{R})^3$ and $\omega_k^\ell \leq \omega_{k+1}^\ell$ for all $k \geq 1$, is a countable infinite family of solutions of the purely elastic problem associated with (4):

$$-\text{div}(A(0)e(u)) = \omega^2 \rho u \text{ in } \Omega. \quad (11)$$

3 The non-linear eigenvalue problem

Problem (4) can be cast as a generalized eigenvalue problem

$$\mathcal{T}(\omega)u = 0 \quad (12)$$

where $\mathcal{T}(\omega)$ is a linear operator depending (non-linearly) on a parameter ω . A solution $u \neq 0$ will exist only for some particular values of ω (also called eigenvalues).

We devote this section to the study of the characterization of the solutions of (4) and (6). We prove in particular that the underlying spectrum of the aforementioned problems is discrete. This feature is of paramount importance since a continuous spectrum or an accumulation point in the spectrum may lead to spurious eigenvalues in numerical applications.

3.1 Preliminary results

Let \mathbb{V} and \mathbb{W} be two complex Hilbert spaces with \mathbb{V} compactly embedded in \mathbb{W} . Let also $\{\mathcal{E}_\omega\}_{\omega \in \mathbb{D}}$, with $\mathbb{D} \subset \mathbb{C}$ open bounded, be a family of complex applications $\mathcal{E}_\omega : \mathbb{V} \times \mathbb{V} \rightarrow \mathbb{C}$.

Definition 3.1 (Sesquilinear form). *We say that $\{\mathcal{E}_\omega\}_{\omega \in \mathbb{D}}$ is a family of sesquilinear forms if for each ω*

1. $\mathcal{E}_\omega(u_1 + u_2, v_1 + v_2) = \mathcal{E}_\omega(u_1, v_1) + \mathcal{E}_\omega(u_1, v_2) + \mathcal{E}_\omega(u_2, v_1) + \mathcal{E}_\omega(u_2, v_2)$,
2. $\mathcal{E}_\omega(\alpha v_1, \beta v_2) = \alpha \bar{\beta} \mathcal{E}_\omega(v_1, v_2)$,

for all $u_1, u_2, v_1, v_2 \in \mathbb{V}$ and all $\alpha, \beta \in \mathbb{C}$. $\bar{\beta}$ is the complex conjugate of β .

Definition 3.2 (Continuous form). *We say that $\{\mathcal{E}_\omega\}_{\omega \in \mathbb{D}}$ is a family of continuous forms if there exists a function $d : \mathbb{D} \rightarrow \mathbb{R}^+$ such that*

$$|\mathcal{E}_\omega(v_1, v_2)| \leq d(\omega) \|v_1\|_{\mathbb{V}} \|v_2\|_{\mathbb{V}}, \forall v_1, v_2 \in \mathbb{V}. \quad (13)$$

We will suppose additionally that the function $d(\omega)$ is continuous in $\bar{\mathbb{D}}$ (thus bounded).

Definition 3.3 (Coercive form). *We say that $\{\mathcal{E}_\omega\}_{\omega \in \mathbb{D}}$ is a family of coercive forms if there exists a function $c : \mathbb{D} \rightarrow \mathbb{R}^+$ such that*

$$|\mathcal{E}_\omega(v, v)| \geq c(\omega) \|v\|_{\mathbb{V}}^2, \forall v \in \mathbb{V}. \quad (14)$$

We will suppose additionally that the function $c(\omega)$ is continuous in $\bar{\mathbb{D}}$ (thus bounded).

From now on, we will assume that $\{\mathcal{E}_\omega\}_{\omega \in \mathbb{D}}$ is a family of continuous coercive sesquilinear forms with continuous bounds.

Proposition 3.1. *For each $\omega \in \mathbb{D}$, define the operators $\mathcal{G}_\omega, \mathcal{G}_\omega^\dagger : \mathbb{W} \rightarrow \mathbb{W}$ such that given $g \in \mathbb{W}$, $\mathcal{G}_\omega(g)$ and $\mathcal{G}_\omega^\dagger(g)$ are respectively the solutions of*

$$\mathcal{E}_\omega(\mathcal{G}_\omega(g), v) = \langle g, v \rangle_{\mathbb{W}}, \forall v \in \mathbb{V}, \quad (15a)$$

$$\mathcal{E}_\omega(v, \mathcal{G}_\omega^\dagger(g)) = \langle g, v \rangle_{\mathbb{W}}, \forall v \in \mathbb{V}. \quad (15b)$$

Then for each $\omega \in \mathbb{D}$, the operators $\mathcal{G}_\omega, \mathcal{G}_\omega^\dagger$ are well-defined and compact.

Proof. We only give the proof for \mathcal{G}_ω since the argument is analogous for $\mathcal{G}_\omega^\dagger$. According to (13) and (14), we can apply the Lax-Milgram theorem to (15a) so for a given $g \in \mathbb{W}$, there exists a unique solution $\mathcal{G}_\omega(g) \in \mathbb{V} \subset \mathbb{W}$. Furthermore, since \mathbb{V} is compactly embedded in \mathbb{W} , there exists a constant $b > 0$ such that

$$b \|\mathcal{G}_\omega(g)\|_{\mathbb{W}} \leq \|\mathcal{G}_\omega(g)\|_{\mathbb{V}},$$

so the operator \mathcal{G}_ω is continuous with

$$\|\mathcal{G}_\omega(g)\|_{\mathbb{W}} \leq \frac{d(\omega)}{bc(\omega)} \|g\|_{\mathbb{W}}, \quad (16)$$

thanks to the Lax-Milgram estimate of (15a). The compactness of the operator $\mathcal{G}_\omega : \mathbb{W} \rightarrow \mathbb{W}$ is finally achieved invoking the compactness of the embedding $\mathbb{V} \hookrightarrow \mathbb{W}$. \square

Proposition 3.2. *Assume that for every $v_1, v_2 \in \mathbb{V}$, the application $\omega \in \mathbb{C} \rightarrow \mathcal{E}_\omega(v_1, v_2) \in \mathbb{C}$ is holomorphic in \mathbb{D} and for ω fixed, the first and second derivative applications of \mathcal{E}_ω , denoted respectively as*

$$\partial_\omega \mathcal{E}_\omega : \mathbb{V} \times \mathbb{V} \rightarrow \mathbb{C}, \quad \partial_\omega^2 \mathcal{E}_\omega : \mathbb{V} \times \mathbb{V} \rightarrow \mathbb{C},$$

are continuous sesquilinear forms with continuous bounds. Then the set of operators $\{\mathcal{G}_\omega\}_{\omega \in \mathbb{D}}$ defined in (15a) is holomorphic in the sense that for every $v_1, v_2 \in \mathbb{W}$ the application

$$\omega \in \mathbb{C} \rightarrow \langle \mathcal{G}_\omega(v_1), v_2 \rangle_{\mathbb{W}} \in \mathbb{C} \quad (17)$$

is holomorphic within \mathbb{D} .

Proof. We will prove that for every fixed $\omega_0 \in \mathbb{D}$, the application (17) is differentiable at ω_0 . Let $p_{\omega_0} \in \mathbb{V}$ be the solution of

$$\mathcal{E}_{\omega_0}(p_{\omega_0}, v) = -\partial_{\omega}\mathcal{E}_{\omega_0}(\mathcal{G}_{\omega_0}(v_1), v), \quad \forall v \in \mathbb{V} \quad (18)$$

for a given $v_1 \in \mathbb{V}$. The existence and uniqueness of p_{ω_0} stems from the Lax-Milgram theorem according to (13), (14) and the continuity of the operator $\partial_{\omega}\mathcal{E}_{\omega_0}$. Let $\Delta\omega \in \mathbb{C}$ be small enough so $\omega_0 + \Delta\omega \in \mathbb{D}$. Then (17) is differentiable with

$$\lim_{\Delta\omega \rightarrow 0} \left| \left\langle \mathcal{G}_{\omega_0 + \Delta\omega}(v_1), v_2 \right\rangle_{\mathbb{W}} - \left\langle \mathcal{G}_{\omega_0}(v_1), v_2 \right\rangle_{\mathbb{W}} - \Delta\omega \left\langle p_{\omega_0}(v_1), v_2 \right\rangle_{\mathbb{W}} \right| = 0. \quad (19)$$

Indeed

$$\begin{aligned} & \left| \left\langle \mathcal{G}_{\omega_0 + \Delta\omega}(v_1), v_2 \right\rangle_{\mathbb{W}} - \left\langle \mathcal{G}_{\omega_0}(v_1), v_2 \right\rangle_{\mathbb{W}} - \Delta\omega \left\langle p_{\omega_0}(v_1), v_2 \right\rangle_{\mathbb{W}} \right| \\ &= \left| \left\langle \mathcal{G}_{\omega_0 + \Delta\omega}(v_1) - \mathcal{G}_{\omega_0}(v_1) - \Delta\omega p_{\omega_0}(v_1), v_2 \right\rangle_{\mathbb{W}} \right| \\ &= \left| \left\langle v_2, \mathcal{G}_{\omega_0 + \Delta\omega}(v_1) - \mathcal{G}_{\omega_0}(v_1) - \Delta\omega p_{\omega_0}(v_1) \right\rangle_{\mathbb{W}} \right| \\ &= \left| \mathcal{E}_{\omega_0 + \Delta\omega} \left(\mathcal{G}_{\omega_0 + \Delta\omega}(v_1) - \mathcal{G}_{\omega_0}(v_1) - \Delta\omega p_{\omega_0}(v_1), \mathcal{G}_{\omega_0 + \Delta\omega}^{\dagger}(v_2) \right) \right| \\ &\leq O(|\Delta\omega|^2 \|v_1\|_{\mathbb{V}} \|v_2\|_{\mathbb{V}}), \end{aligned} \quad (20)$$

so taking the limit of the aforementioned inequality when $\Delta\omega \rightarrow 0$ yields (19). The equality (20) derives from (15b). Since we assume that the application $\omega \rightarrow \mathcal{E}_{\omega}(v_1, v_2)$ is holomorphic for $\omega \in \mathbb{D}$ and the continuity and coercivity bounds of $\mathcal{E}_{\omega}, \partial_{\omega}\mathcal{E}_{\omega}, \partial_{\omega}^2\mathcal{E}_{\omega}$, are bounded in \mathbb{D} , the inequality (21) results from developing $\mathcal{E}_{\omega + \Delta\omega}$ as a Taylor expansion of order two around $\omega = \omega_0$ and applying (15a), (16) and (18). \square

3.2 Main result

The main conclusion of this section corresponds to the application of a result of standard analytical perturbation theory of compact operators. This theorem describes locally the eigenvalues of a general non-linear eigenvalue problem

Theorem 3.1 ([15], chapter VII, Th. 1.9). *Let $\mathcal{S}(\omega)$ be a family of compact operators (for each ω fixed) and holomorphic with respect to $\omega \in \mathbb{D} \subset \mathbb{C}$ bounded. Define ω as a singular point if 1 is an eigenvalue of $\mathcal{S}(\omega)$. Then either all $\omega \in \mathbb{D}$ are singular points or there are only a finite number of singular points in each compact subset of \mathbb{D} .*

Theorem 3.2. *Suppose that the weak formulation of (12) has the following structure on ω*

$$\mathcal{E}_{\omega}(u, v) - \omega^2 \langle u, v \rangle_{\mathbb{W}} = 0, \quad \forall v \in \mathbb{V}, \quad (22)$$

and assume the same hypothesis as Proposition 3.1 and Proposition 3.2. Furthermore suppose that $0 \in \mathbb{D}$ and \mathcal{E}_0 hermitian positive definite. Then there are only a finite number of eigenvalues of (22) in \mathbb{D} .

Proof. Define the operator $\mathcal{S}_{\omega} : \mathbb{W} \rightarrow \mathbb{W}$ as

$$\mathcal{S}_{\omega} = \omega^2 \mathcal{G}_{\omega}$$

Then according to Proposition 3.1 and Proposition 3.2, $\{\mathcal{S}_{\omega}\}_{\omega \in \mathbb{C}}$ is a family of compact operators and \mathcal{S}_{ω} is holomorphic with respect to ω in \mathbb{D} . Furthermore, if a given $\omega \neq 0$ is an eigenvalue of (22), then 1 is an eigenvalue of \mathcal{S}_{ω} according to (15a). If every $\omega \in \mathbb{D} \setminus \{0\}$ fulfilled the aforementioned condition, then since \mathbb{D} is open, there would be a sequence $\{z_j\}_{j \in \mathbb{N}} \in \mathbb{D}$ and $\{v_j\}_{j \in \mathbb{N}} \in \mathbb{V}$ with $\|v_j\|_{\mathbb{V}} = 1$, such that $z_j \rightarrow 0$ when $j \rightarrow \infty$ and

$$|\mathcal{E}_{z_j}(v_j, v_j)| = |z_j^2 \langle v_j, v_j \rangle_{\mathbb{W}}| \leq |z_j^2|, \quad \forall j \in \mathbb{N}. \quad (23)$$

Now since \mathcal{E}_0 is hermitian positive definite, all its eigenvalues are real positive. In particular, its first eigenvalue (that we denote as λ_1) satisfies the Rayleigh quotient

$$\min_{v \in \mathbb{V}, \|v\|_{\mathbb{V}}=1} \mathcal{E}_0(v, v) = \lambda_1 > 0.$$

Then, since \mathcal{E}_ω is holomorphic and (23)

$$\mathcal{E}_0(v_j, v_j) \leq |\mathcal{E}_0(v_j, v_j) - \mathcal{E}_{z_j}(v_j, v_j)| + |\mathcal{E}_{z_j}(v_j, v_j)| = O(|z_j|)$$

and we obtain a contradiction for j large enough. The desired result finally stems from Theorem 3.1. \square

We give an application of the above theorem to the 3D viscoelastic and UCLD plate vibration problems

Corollary 3.1. *Suppose that the complex elastic tensors $A(\omega)$ and $D(\omega)$ in (4) and (6) respectively, are holomorphic with respect to ω for $\omega \in \mathbb{D} \subset \mathbb{C}$ bounded. Suppose also that $0 \in \mathbb{D}$ and $A(0), D(0)$ are hermitian positive definite. Then problems (4) and (6) possess only a finite number of eigenvalues in \mathbb{D} .*

Proof. The result derives from Theorem 3.2 by considering

$$\mathcal{E}_\omega(u, v) = \int_{\Omega} A(\omega)e(u) : e(\bar{v})dx, \mathbb{V} = \{v \in H^1(\Omega; \mathbb{C})^3 : v = 0 \text{ on } \Gamma_D\}, \mathbb{W} = L^2(\Omega; \mathbb{C})^3$$

in problem (4) and

$$\mathcal{E}_\omega(w, \zeta) = \int_{\mathcal{O}} D(\omega)\nabla^2 w : \nabla^2 \bar{\zeta}dx, \mathbb{V} = \{\zeta \in H^2(\mathcal{O}; \mathbb{C}) : \zeta = 0, \nabla\zeta = 0 \text{ on } \Gamma_D\}, \mathbb{W} = L^2(\mathcal{O}; \mathbb{C})$$

in problem (6). \square

4 Sensitivity analysis of ω_1 with respect the shape Ω

We dedicate this section to the study of the shape differentiability of ω_1 and eigenvectors (u_1, w_1) , solutions of (4) and (6) respectively. Nevertheless all results remain valid for $k \geq 2$ by replacing (ω_1, u_1, w_1) with (ω_k, u_k, w_k) .

4.1 Differentiability of ω_1

Theorem 4.1. *Suppose Ω measurable and bounded and $\omega_1(\Omega)$ simple. Then the first eigenfrequency $\omega_1(\Omega)$, $u_1(\Omega)$ (for $d = 3$) and $w_1(\Omega)$ (for $d = 2$) are shape differentiable at 0.*

We omit the proof since it corresponds to an adaptation of the result exhibited in [11] chapter 5, page 210.

4.2 Shape derivative of a 3D viscoelastic structure

Define the space $V = \{v \in H^1(\Omega; \mathbb{C})^3 : v = 0 \text{ on } \Gamma_D\}$.

Theorem 4.2. *Let $(\omega_1, u_1) \in \mathbb{C} \times V$ be the solutions of the eigenvalue problem (4) and ω_1 simple. Also let $A^H(\omega_1) = \overline{A(\omega_1)^T}$ be the conjugate transpose tensor of A and introduce the adjoint eigenvector $p_1 \in V$ solution of*

$$\int_{\Omega} A^H(\omega_1)e(p) : e(\bar{v})dx = \omega^2 \int_{\Omega} \rho(p \cdot \bar{v})dx, \quad \forall v \in V, \quad (24)$$

with $\int_{\Omega} \rho|p_1|^2 dx = 1$ and $\omega^2 = \overline{\omega_1^2}$. Then:

$$\omega_1' = - \frac{\int_{\partial\Omega} \theta \cdot n \left(\omega_1^2 \rho(u_1 \cdot \bar{p}_1) - A(\omega_1)e(u_1) : e(\bar{p}_1) \right) ds}{\int_{\Omega} \left(2\omega_1 \rho(u_1 \cdot \bar{p}_1) - \partial_{\omega} A(\omega_1)e(u_1) : e(\bar{p}_1) \right) dx}. \quad (25)$$

Proof. As mentioned in the previous section, the fact that ω_1 is simple ensures that $\omega_1(\Omega)$ and $u_1(\Omega)$ are shape-differentiable. Thus we can directly derive both sides of the variational formulation of (4)

$$\int_{\Omega} A(\omega_1)e(u_1) : e(\bar{v})dx = \omega_1^2 \int_{\Omega} \rho(u_1 \cdot \bar{v})dx, \quad \forall v \in V \quad (26)$$

Taking $\theta \in W^{1,\infty}(\mathbb{R}^3, \mathbb{R}^3)$ with $\theta = 0$ on $\Gamma_N \cup \Gamma_D$:

$$\begin{aligned} & \int_{\partial\Omega} A(\omega_1)e(u_1) : e(\bar{v})(\theta \cdot n)ds + \omega_1'(\theta) \int_{\Omega} (\partial_{\omega}A)e(u_1) : e(\bar{v})dx + \int_{\Omega} A(\omega_1)e(u_1'(\theta)) : e(\bar{v})dx \\ & = 2\omega_1\omega_1'(\theta) \int_{\Omega} \rho(u_1 \cdot \bar{v})dx + \omega_1^2 \int_{\Omega} \rho(u_1' \cdot \bar{v})dx + \omega_1^2 \int_{\partial\Omega} \rho(u_1 \cdot \bar{v})(\theta \cdot n)ds \end{aligned} \quad (27)$$

Then taking $v = p_1$ in (27) yields

$$\begin{aligned} & \int_{\partial\Omega} A(\omega_1)e(u_1) : e(\bar{p}_1)(\theta \cdot n)ds + \omega_1'(\theta) \int_{\Omega} (\partial_{\omega}A)e(u_1) : e(\bar{p}_1)dx \\ & = 2\omega_1\omega_1'(\theta) \int_{\Omega} \rho(u_1 \cdot \bar{p}_1)dx + \omega_1^2 \int_{\partial\Omega} \rho(u_1 \cdot \bar{p}_1)(\theta \cdot n)ds, \end{aligned}$$

from which (25) follows. □

Remark 4.1. When the tensor A is independent from the frequency ω , we recover the well-known formula [2] for the derivative:

$$\omega_1' = - \frac{\int_{\partial\Omega} \theta \cdot n \left(\omega_1^2 \rho(u_1 \cdot \bar{p}_1) - A(\omega_1)e(u_1) : e(\bar{p}_1) \right) ds}{\int_{\Omega} 2\omega_1 \rho(u_1 \cdot \bar{p}_1) dx}$$

Furthermore if A is real then the problem becomes self-adjoint (i.e. $p_1 = u_1$).

4.3 Shape derivative of a composite sandwich structure

We refer to the notations given in Section 2.2. Define a bounded working domain $\mathcal{O} \subset \mathbb{R}^2$ and an admissible shape $\Omega \subset \mathcal{O}$ occupied by a viscoelastic damping treatment. Within this framework, (6) can be formulated as a multi-phase problem. As mentioned in [1], a sharp interface between the different phases leads to numerical difficulties that can be avoided by considering a smeared or diffuse interface approach. We follow herein this smoothed formulation. Let D and ρ be the smooth interpolations between D_g, D_p , (with respective surface densities ρ_g, ρ_p) occupying each one Ω and $\mathcal{O} \setminus \bar{\Omega}$ respectively, defined as

$$\begin{aligned} D &= D_g - H_{\varepsilon}(d_{\Omega})\Delta D, & \Delta D &:= (D_g - D_p), \\ \rho &= \rho_g - H_{\varepsilon}(d_{\Omega})\Delta \rho, & \Delta \rho &:= (\rho_g - \rho_p), \end{aligned} \quad (28)$$

where $H_{\varepsilon}(r) : \mathbb{R} \rightarrow [0, 1]$ is a smooth approximation of the Heaviside function

$$H_{\varepsilon}(r) = \begin{cases} 0 & \text{if } r < -\varepsilon, \\ \frac{1}{2} \left(1 + \frac{r}{\varepsilon} + \frac{1}{\pi} \sin\left(\frac{\pi r}{\varepsilon}\right) \right) & \text{if } -\varepsilon \leq r \leq \varepsilon, \\ 1 & \text{if } r > \varepsilon, \end{cases} \quad (29)$$

and $d_{\Omega}(x) : \mathbb{R}^d \rightarrow \mathbb{R}$ the signed distance function associated with Ω

$$d_{\Omega}(x) = \begin{cases} 0 & \text{if } x \in \partial\Omega, \\ - \min_{x_I \in \partial\Omega} |x - x_I| & \text{if } x \in \Omega, \\ \min_{x_I \in \partial\Omega} |x - x_I| & \text{if } x \in \mathcal{O} \setminus \bar{\Omega}. \end{cases}$$

Define the space $W = \{\zeta \in H^2(\mathcal{O}; \mathbb{C}) : \zeta = 0, \nabla\zeta = 0 \text{ on } \Gamma_D\}$.

Theorem 4.3. Let $(\omega_1, w_1) \in \mathbb{C} \times W$ be the solutions of the eigenvalue problem (6) and ω_1 simple. Also let $D^H(\omega_1) = \overline{D(\omega_1)^T}$ be the conjugate transpose tensor of D and introduce the adjoint eigenvector $q_1 \in W$ solution of

$$\int_{\mathcal{O}} D^H(\omega_1) \nabla^2 q : \nabla^2 \bar{\zeta} dx = \omega^2 \int_{\mathcal{O}} \rho(q \cdot \bar{\zeta}) dx, \quad \forall \zeta \in W, \quad (30)$$

with $\int_{\mathcal{O}} \rho |q_1|^2 dx = 1$ and $\omega^2 = \overline{\omega_1^2}$. Then:

$$\omega'_1 = - \frac{\int_{\mathcal{O}} \partial_r H_\varepsilon(d_\Omega) \left(\omega_1^2 \Delta \rho(w_1 \cdot \bar{q}_1) - \Delta D(\omega_1) \nabla^2 w_1 : \nabla^2 \bar{q}_1 \right) \theta(P_{\partial\Omega}(x)) \cdot n(P_{\partial\Omega}(x)) dx}{\int_{\mathcal{O}} \left(2\omega_1 \rho(w_1 \cdot \bar{q}_1) - \partial_\omega D(\omega_1) \nabla^2 w_1 : \nabla^2 \bar{q}_1 \right) dx}, \quad (31)$$

where $P_{\partial\Omega}(x)$ is the projection of x onto $\partial\Omega$.

Proof. In the same way as Theorem 4.2, we derive both sides of the variational formulation of (4) but this time within the fixed domain \mathcal{O}

$$\int_{\mathcal{O}} D(\omega_1) \nabla^2 w_1 : \nabla^2 \bar{\zeta} dx = \omega_1^2 \int_{\mathcal{O}} \rho(w_1 \cdot \bar{\zeta}) dx, \quad \forall \bar{\zeta} \in W.$$

Taking $\theta \in W^{1,\infty}(\mathbb{R}^3, \mathbb{R}^3)$ with $\theta = 0$ on $\partial\mathcal{O}$

$$\begin{aligned} & \int_{\mathcal{O}} D'(\theta)(\omega_1) \nabla^2 w_1 : \nabla^2 \bar{\zeta} dx + \omega'_1(\theta) \int_{\mathcal{O}} \partial_\omega D \nabla^2 w_1 : \nabla^2 \bar{\zeta} dx + \int_{\mathcal{O}} D(\omega_1) \nabla^2 w'_1(\theta) : \nabla^2 \bar{\zeta} dx \\ &= 2\omega_1 \omega'_1(\theta) \int_{\mathcal{O}} \rho(w_1 \cdot \bar{\zeta}) dx + \omega_1^2 \int_{\mathcal{O}} \rho'(w_1 \cdot \bar{\zeta}) dx + \omega_1^2 \int_{\mathcal{O}} \rho'(w_1 \cdot \bar{\zeta}) dx. \end{aligned}$$

Then taking $\zeta = q_1$ in the above equation yields

$$\begin{aligned} & \int_{\mathcal{O}} D'(\theta)(\omega_1) \nabla^2 w_1 : \nabla^2 \bar{q}_1 dx + \omega'_1(\theta) \int_{\mathcal{O}} \partial_\omega D \nabla^2 w_1 : \nabla^2 \bar{q}_1 dx \\ &= 2\omega_1 \omega'_1(\theta) \int_{\mathcal{O}} \rho(w_1 \cdot \bar{q}_1) dx + \omega_1^2 \int_{\mathcal{O}} \rho'(w_1 \cdot \bar{q}_1) dx, \end{aligned}$$

so

$$\omega'_1 = - \frac{\int_{\mathcal{O}} \left(\omega_1^2 \rho'(\theta)(w_1 \cdot \bar{q}_1) - D'(\theta)(\omega_1) \nabla^2 w_1 : \nabla^2 \bar{q}_1 \right) dx}{\int_{\mathcal{O}} \left(2\omega_1 \rho(w_1 \cdot \bar{q}_1) - \partial_\omega D(\omega_1) \nabla^2 w_1 : \nabla^2 \bar{q}_1 \right) dx}. \quad (32)$$

According to (28), the shape derivatives ρ' and D' read

$$\begin{aligned} \rho'(\theta)(x) &= -\partial_r H_\varepsilon(d_\Omega) d'_\Omega(\theta)(x) \Delta \rho, \\ D'(\theta)(x, \omega_1) &= -\partial_r H_\varepsilon(d_\Omega) d'_\Omega(\theta)(x) \Delta D(\omega_1), \end{aligned}$$

where $d'_\Omega(\theta)(x) = -\theta(P_{\partial\Omega}(x)) \cdot n(P_{\partial\Omega}(x))$ is the shape derivative of the signed distance function at x (Proposition 3.5. [1]). \square

Obtaining a descent direction from (31) is not necessarily easy and we would prefer to recover the classical shape derivative structure of a surface integral on the interface.

Corollary 4.1. *Suppose that the interface is roughly plane (i.e. the principal curvatures can be neglected) and the thickness parameter ε of the diffuse interface is small. Then a good approximation of (31) is*

$$\omega'_1 \approx - \frac{\int_{\Gamma} \theta \cdot n \left(\omega_1^2 \Delta \rho(w_1 \cdot \bar{q}_1) - \Delta D(\omega_1) \nabla^2 w_1 : \nabla^2 \bar{q}_1 \right) ds}{\int_{\mathcal{O}} \left(2\omega_1 \rho(w_1 \cdot \bar{q}_1) - \partial_\omega D(\omega_1) \nabla^2 w_1 : \nabla^2 \bar{q}_1 \right) dx}, \quad (33)$$

where $\Gamma = \partial\Omega \cap \text{int}(\mathcal{O})$.

For the proof consult [1].

5 Level-set method for topology optimization

From the previous sections we have all the necessary theoretical ingredients to introduce a gradient method for the minimization of an objective function $J(\Omega)$. The general form of its shape derivative is

$$J'(\Omega)(\theta) = \int_{\partial\Omega} (\theta \cdot n) V ds,$$

where the function $V(x)$ is given in (25) and (33). Supposing V regular enough so it can be naturally extended to \mathbb{R}^d , a descent direction is found by defining the vector field

$$\theta = -Vn$$

and we update the shape Ω as

$$\Omega_t = (Id + t\theta)\Omega,$$

where $t > 0$ is a small descent step. Formally we obtain

$$J(\Omega_t) = J(\Omega) - t \int_{\partial\Omega} V^2 ds + O(t^2)$$

which guarantees the decrease of the objective function. We remark that if V turns out to be not regular enough (as it is the case for some objective functions) there are other possible choices for the definition of the descent direction [6].

First introduced in [19], the level-set method is a technique for capturing interfaces which are implicitly defined via the zero level-set of an auxiliary function. In particular, this method has been successfully applied to topology optimization problems. Let the bounded domain $\mathcal{O} \subset \mathbb{R}^d$ be the working domain in which all admissible shapes Ω are included. In numerical practice, the domain \mathcal{O} will be meshed once and for all. We parametrize the boundary of Ω by means of a level-set function ψ defined over \mathcal{O} such that

$$\begin{cases} \psi(x) = 0 & \text{if } x \in \partial\Omega, \\ \psi(x) < 0 & \text{if } x \in \Omega, \\ \psi(x) > 0 & \text{if } x \in (\mathcal{O} \setminus \overline{\Omega}). \end{cases} \quad (34)$$

Under the action of a normal vector field $V(t, x)n(x)$, the shape Ω evolves according to the Hamilton-Jacobi equation

$$\frac{\partial\psi}{\partial t}(t, x) + V(t, x)|\nabla\psi(t, x)| = 0, \quad \forall t, \forall x \in \mathcal{O}. \quad (35)$$

Equation (35) is posed in the whole reference domain \mathcal{O} , and not only on the boundary $\partial\Omega$, if the velocity V is known everywhere (as will be the case in the sequel). Transporting ψ by (35) is analogous to moving the boundary of $\partial\Omega$ (the zero level-set of ψ) along the direction V .

A common choice of boundary condition for (35) is

$$\frac{\partial\psi}{\partial n} = 0 \text{ on } \partial\mathcal{O}.$$

As mentioned in [2], this boundary condition is easy to implement since there is no fixed value to assign for ψ at the boundary, and it also allows the solution of (35) to satisfy a maximum principle. More precisely, new inclusions (or holes) in Ω can appear only by advecting the zero level-set of ψ which changes its topology and cannot come from outside the domain \mathcal{O} because of spurious negative values created by the boundary conditions.

The numerical solution of (35) is computed with a second order explicit upwind scheme [22] on a Cartesian grid. Since this scheme is explicit in time, the time stepping must satisfy a CFL condition.

Because of the advection process or numerical diffusion, the level-set function may become too flat or too steep leading to large errors either in the location of its zero level set or in the evaluation of its gradient by finite differences. Therefore, it is usual to regularize it periodically by solving the following problem

$$\begin{cases} \frac{\partial\psi}{\partial t}(t, x) + \text{sign}(\psi_0)(|\nabla\psi(t, x)| - 1) = 0, & \forall t, \forall x \in \mathcal{O} \\ \psi(t = 0, x) = \psi_0(x) & \forall x \in \mathcal{O}, \end{cases} \quad (36)$$

which admits as a stationary solution the signed distance to the initial interface $\psi_0(x) = 0$.

6 Numerical analysis

6.1 Material properties

In order to extend the state equation (4) to the whole domain \mathcal{O} , we use the same “ersatz material” approach as [3]. This approach amounts to filling the holes $\mathcal{O} \setminus \Omega$ by a weak phase mimicking void but avoiding the singularity of the rigidity matrix. We define an elasticity tensor $A^*(x)$, which is a mixture of A in Ω and of the weak material mimicking holes in $\mathcal{O} \setminus \Omega$, as

$$A^*(x) = \chi_A(x)A, \quad \chi_A(x) = \begin{cases} 1, & \text{if } x \in \Omega, \\ \delta_A, & \text{if } x \in \mathcal{O} \setminus \Omega. \end{cases} \quad (37)$$

We also need to apply the same procedure for the material density by introducing a mixture density

$$\rho^*(x) = \chi_\rho(x)\rho, \quad \chi_\rho(x) = \begin{cases} 1 & \text{if } x \in \Omega, \\ \delta_\rho & \text{if } x \in \mathcal{O} \setminus \Omega. \end{cases} \quad (38)$$

For eigenfrequency optimization making a correct choice for the threshold parameters δ_A and δ_ρ is always delicate since a bad combination can yield spurious eigenmodes localized in the ersatz material.

In the case of the composite sandwich structure equation (6), the tensor D and the density ρ are evaluated according to the smooth multi-phase approximation (28) considering $d_\Omega = \psi$, i.e. the current level-set function. Indeed the level-set function ψ is periodically reinitialized through (36). We set $\varepsilon = 1.5\Delta x$ in (29) where Δx is the characteristic size of the computation mesh. We remark that in the multi-phase framework we do not need an ersatz material since the whole domain \mathcal{O} is covered by the base plate material which makes the rigidity matrix of the composite sandwich always non-singular, no matter the shape of the damping layer.

6.2 Solving the discrete non-linear eigenvalue problem

Denote as

$$\mathcal{T}_h(\omega) \cdot u_h = 0, \quad u_h \in V_h \quad (39)$$

the matrix representation of the discretization of problem (12) that stems from the weak (or variational) formulation of (4) (for the functional space notation V_h refer to (26)). Among the various methods to solve (39) (consult for instance [21]), we simply elect to apply Newton’s method to the extended system

$$F_z(\omega, u_h) = \begin{pmatrix} \mathcal{T}_h(\omega) \cdot u_h \\ \bar{z} \cdot u_h - 1 \end{pmatrix} = 0, \quad (40)$$

where $z \in V_h$ is an arbitrary vector, fixed once and for all, such that $\|z\| = 1$ and $\bar{z} \cdot u_h^* \neq 0$, being u_h^* the exact eigenvector of (39). Hence the second equation in (40) represents a normalization condition on u_h . The numerical solution $(\omega_1^\ell, u_1^\ell)$ obtained by FEM discretization of the problem (11) is chosen as the initial value (ω^0, u_h^0) and $z = u_h^0$. The Newton equation of (40)

$$F_z(\omega^n, u_h^n) + \partial F_z(\omega^n, u_h^n) \begin{pmatrix} \omega^{n+1} - \omega^n \\ u_h^{n+1} - u_h^n \end{pmatrix} = 0$$

gives the following update rules:

$$\omega^{n+1} = \omega^n - \frac{1}{\bar{z} \cdot \mathcal{T}_h^{-1}(\omega^n) \cdot \mathcal{T}'_h(\omega^n) \cdot u_h^n},$$

$$u_h^{n+1} = (\omega^n - \omega^{n+1}) \mathcal{T}_h^{-1}(\omega^n) \cdot \mathcal{T}'_h(\omega^n) \cdot u_h^n,$$

where the matrices $\mathcal{T}_h^{-1}(\omega^n)$ and $\mathcal{T}'_h(\omega^n)$ respectively stand for the inverse and the derivative with respect to ω of the FEM matrix $\mathcal{T}_h(\omega^n)$. We iterate until $|\omega^{n+1} - \omega^n|/|\omega^n| < tol$ with $tol \ll 1$.

6.3 Computing a descent direction

The gradient of the loss factor

$$\eta(\Omega) = \frac{\text{Im}(\omega_1^2)}{\text{Re}(\omega_1^2)},$$

can be derived from the formulas given in Sections 4.2 and 4.3. Applying the product rule

$$\eta' = 2 \frac{\text{Re}(\omega_1^2) \text{Im}(\omega_1 \omega_1') - \text{Im}(\omega_1^2) \text{Re}(\omega_1 \omega_1')}{\text{Re}(\omega_1^2)^2} = 2 \frac{\text{Im}(\overline{\omega_1^2} \omega_1 \omega_1')}{\text{Re}(\omega_1^2)^2} = 2(1 - \eta) \frac{\text{Im}(\omega_1 \omega_1')}{\text{Re}(\omega_1^2)}. \quad (41)$$

6.3.1 3D viscoelastic structure

For a given ω_1 , define the constant

$$\beta(\omega_1) := \int_{\Omega} \left(2\omega_1 \rho (u_1 \cdot \bar{p}_1) - \partial_{\omega} A(\omega_1) e(u_1) : e(\bar{p}_1) \right) dx$$

and the function

$$\gamma(\omega_1)(x) := \omega_1^2 \rho (u_1 \cdot \bar{p}_1) - A(\omega_1) e(u_1) : e(\bar{p}_1).$$

Write (25) as

$$\omega_1' = - \frac{\int_{\partial\Omega} \theta \cdot n \left(\overline{\beta(\omega_1)} \gamma(\omega_1) \right) ds}{|\beta(\omega_1)|^2}.$$

Then since θ and the normal n are real-valued, (41) reads

$$\eta' = - \frac{2(1-\eta)}{\operatorname{Re}(\omega_1^2) |\beta(\omega_1)|^2} \int_{\partial\Omega} (\theta \cdot n) \operatorname{Im} \left(\omega_1 \overline{\beta(\omega_1)} \gamma(\omega_1) \right) ds. \quad (42)$$

The above expression provides directly a normal ascent direction $\theta = Vn$, with

$$V = - \frac{2(1-\eta)}{\operatorname{Re}(\omega_1^2) |\beta(\omega_1)|^2} \operatorname{Im} \left(\omega_1 \overline{\beta(\omega_1)} \gamma(\omega_1) \right).$$

6.3.2 Composite sandwich structure

Following the same development, with the definitions

$$\beta(\omega_1) := \int_{\mathcal{O}} \left(2\omega_1 \rho (w_1 \cdot \bar{q}_1) - \partial_{\omega} D(\omega_1) \nabla^2 w_1 : \nabla^2 \bar{q}_1 \right) dx$$

and

$$\gamma(\omega_1)(x) := \omega_1^2 (\rho_g - \rho_c) (w_1 \cdot \bar{q}_1) - (D_g - D_c)(\omega_1) \nabla^2 w_1 : \nabla^2 \bar{q}_1,$$

the same descent direction (42) applies.

6.4 Test cases

Numerical test cases involving the structure eigenvalues in topology optimization are usually not well-posed since less structure implies a higher eigenfrequency as a result of the ersatz material. Typical remedies are including non-structural masses, defining the problem as a reinforcement problem or imposing a mass equality constraint. For the following test cases we apply the first two solutions.

The 3D and 2D eigenvalue computations are performed using Freefem++ [10] and the 3D results are rendered with XD3D [14].

The chosen viscoelastic properties for the 3D and 2D cases satisfy the holomorphic condition stated in Section 3 (except on a finite number of poles). That being said, the optimization process remains valid for any other viscoelastic material.

6.4.1 3D viscoelastic structure

We optimize a three-dimensional cantilever. The working domain \mathcal{O} is of size $1\text{m} \times 2\text{m} \times 1\text{m}$ (discretized with a $20 \times 20 \times 40$ mesh). A zero displacement boundary condition is imposed on the left side and four cubic cells on the middle of the right side (heavy tip mass) are not subject to optimization and a material density 100 times heavier (see Figures 4 and 5). The viscoelastic material corresponds to 3M ISD112 with complex Young modulus

$$E_c(\omega) = (1 + \nu_c) G_0 \left(1 + \sum_{k=1}^3 \frac{\Delta_k \omega}{\omega - i\Omega_k} \right), G_0 = 0.5\text{MPa}, \quad (43)$$

density $\rho_c^V = 1600 \text{ kg/m}^3$ and Poisson coefficient $\nu_c = 0.5$ (consult [25] for the values of the not listed constants Ω_k and Δ_k). The ersatz material is characterized by the same Poisson's ratio as the viscoelastic material, a smaller Young's modulus by a factor $\delta_A = 10^{-2}$ and a smaller density by a factor $\delta_{\rho} = 10^{-4}$

(see (37) and (38)). The objective function is given as a linear combination of the negative loss factor (since we minimize) and the volume of the structure

$$J(\Omega) = -\eta + \ell \frac{|\Omega|}{|\mathcal{O}|}, \quad (44)$$

where $\ell = 0.01$ is a fixed Lagrange multiplier for the volume constraint. The heavy tip mass is positioned on the rectangular (and not the square) face of the design domain in order to avoid the symmetric bending modes on the X and Y axis. This condition is not necessarily sufficient to enforce the first eigenvalue ω_1 to be simple (our computations are based on this assumption) so we check at each iteration the existence of multiple eigenvectors. The modal loss factors η of the initial and optimal shapes are respectively 0.025 and 0.041.

Remark 6.1. *In this case Ω corresponds to a uniform isotropic viscoelastic structure such that*

$$A(\omega) = f(\omega)A_0,$$

where f is a scalar function and A_0 is a real isotropic material independent of ω (both defined accordingly to equation (43)). Hence solving the problem (4) is equivalent to solving the equation:

$$-\operatorname{div}(A_0 e(u)) = \lambda \rho u \text{ in } \Omega, \quad (45)$$

which has a countable infinite family of solutions $(\lambda_k, u_k)_{k \geq 1}$. The eigenmodes u_k coincide with the eigenmodes of the original viscoelastic problem and we can easily check that $p_k = u_k$, so the optimization problem is self-adjoint. In order to compute the modal loss factor η , we determine the original eigenvalue ω_1 as the solution of the non-linear scalar equation:

$$\omega^2 - f(\omega)\lambda_1 = 0,$$

via Newton's method with the initial value $\omega_1^0 = \lambda_1^{1/2}$.

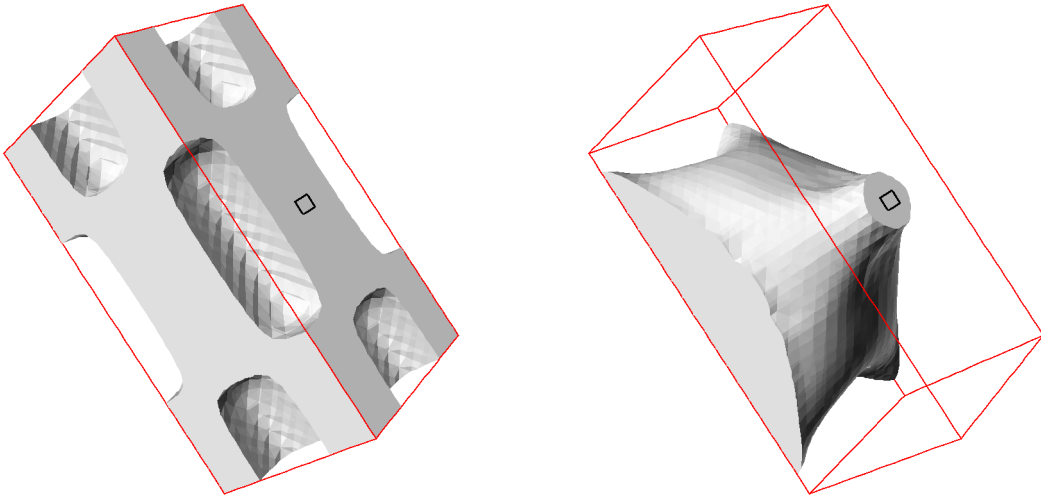


Figure 4: Initial (with a cavity inside) and optimized shapes of a 3D cantilever.

6.4.2 Composite sandwich structure

Now we optimize a square plate \mathcal{O} with all edges clamped ($w = \partial w / \partial n = 0$ on $\partial \mathcal{O}$). The width and the length of the working domain are both 400mm, discretized with a 40×40 mesh. The thickness of the base plate and the damping layer are 8.75mm and 1.25mm, respectively. The base layer is made of aluminum whose Young modulus is $E_p = 69\text{GPa}$, Poisson's coefficient $\nu_p = 0.3$ and volumetric density

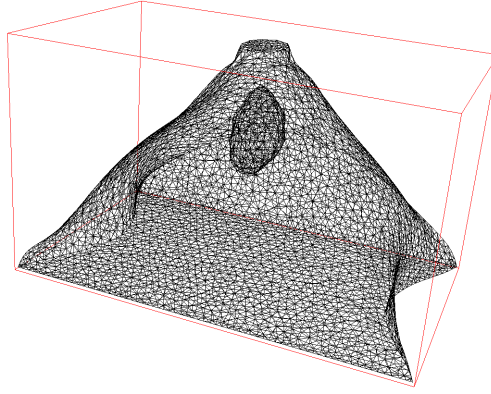


Figure 5: The optimized shape possesses a small inner cavity. If the hole is filled with the viscoelastic material, the value of η remains almost constant (actually it slightly diminishes) so the value of the composite objective function (44) increases. The authors verified that the inner cavity is not present when the whole working domain \mathcal{O} is used as initial shape in the optimization process.

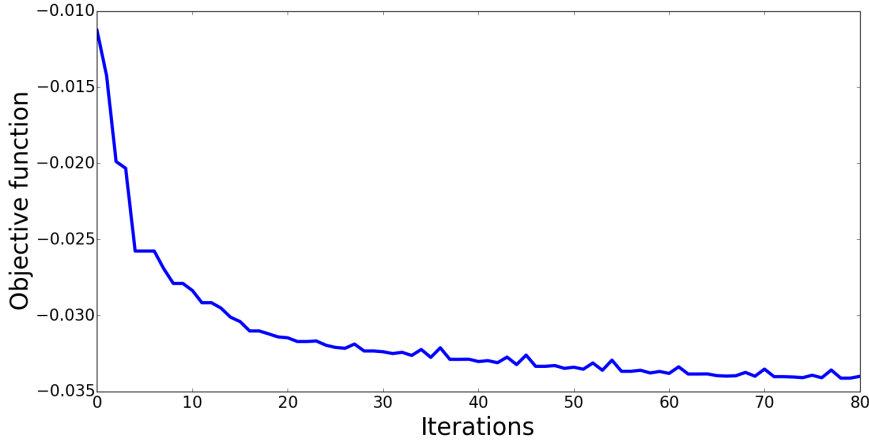


Figure 6: Convergence history for the optimization of the 3D cantilever.

$\rho_p^V = 2760 \text{ kg/m}^3$. The viscoelastic coating corresponds to LD-400, a fractional derivative model material depending on the temperature T with complex Young modulus

$$E_c(\omega) = \frac{a_0 + a_1(i\omega\alpha(T))^\beta}{1 + c_1(i\omega\alpha(T))^\beta} \text{MPa}, \quad (46)$$

density $\rho_c^V = 1524 \text{ kg/m}^3$ and Poisson coefficient $\nu_c = 0.5$. The four parameters $a_0 = 332.2$, $a_1 = 2485.2$, $c_1 = 0.12$, $\beta = 0.47$ and the shift factor $\alpha(T)$ are available in [13]. In our case we will consider the temperature T to be constant and equal to 27°C .

The objective function $J(\Omega)$ is the same that (44) but this time with $\ell = 10^{-1}$. The modal loss factors of the initial and optimized shapes are respectively 1.5×10^{-2} and 2.31×10^{-2} (see Figure 7). We remark that the optimized shape of the viscoelastic treatment coincides with the one obtained in [16] using the SIMP method. The result may not be completely intuitive at first since a significant portion of the damping reinforcement material lays outside the eigenmode largest deflection zone (Figure 8). However, as explained in Section 2.2, the sandwich energy is mainly dissipated as a result of in-plane compression and extension of the damping material under the flexural stress of the base plate. Hence the optimal damping reinforcement material lay-out and the area with the largest extensional strain energy density overlap (see Figure 9).

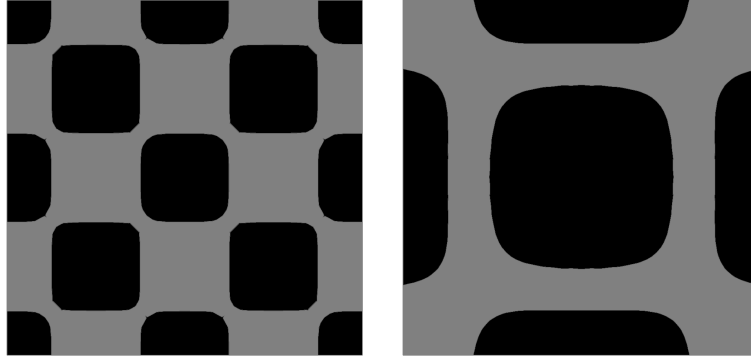


Figure 7: Initial and optimized shapes of the composite plate. The aluminum phase is shown in gray and the (superposed) viscoelastic one in black.

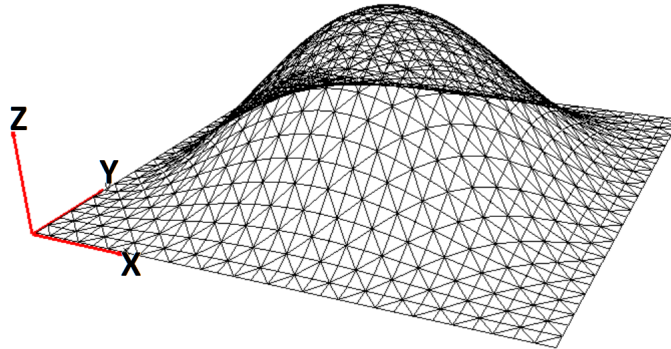


Figure 8: Real part of the eigenmode w_1 for the final shape.

Acknowledgments

This research work was carried out in the framework of IRT SystemX, Paris-Saclay, France, and therefore supported with public funds within the scope of the French Program “Investissements d’Avenir”. The authors also thank the financial support of the industrial partners of the TOP project: Safran, Renault, Airbus Group and ESI Group. We would like additionally to show our gratitude to Julien Cortial who read carefully this article providing a very useful feedback.

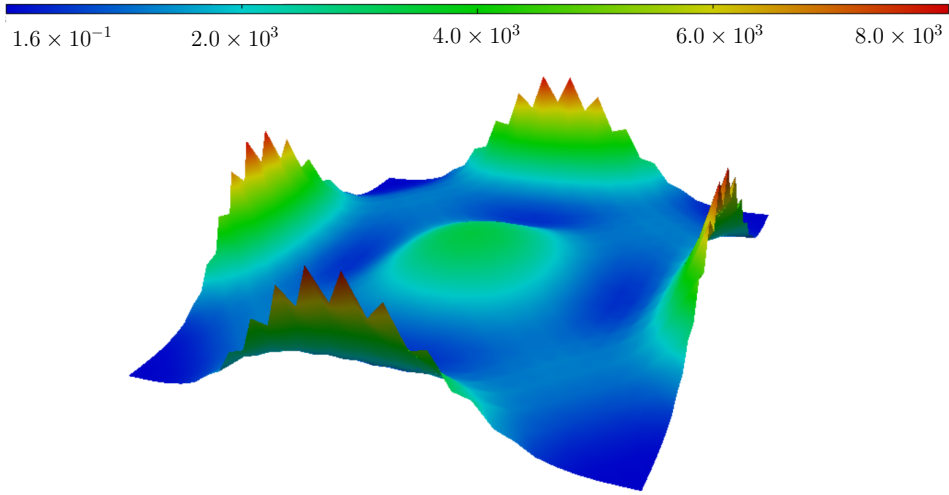


Figure 9: In-plane extensional strain energy density (J/m^2).

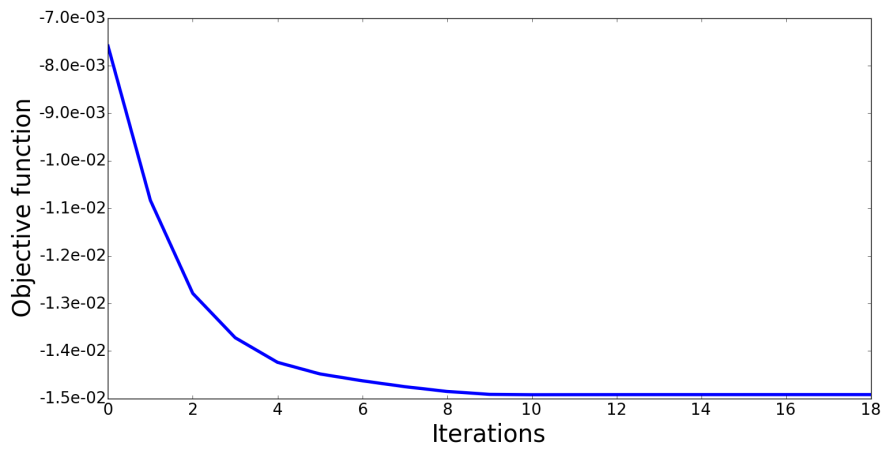


Figure 10: Convergence history for the optimization of the 2D composite sandwich plate.

References

- [1] G. Allaire, C. Dapogny, G. Delgado, and G. Michailidis. Multi-phase structural optimization via a level set method. *ESAIM: Control, Optimisation and Calculus of Variations*, 20(2):576–611, 2014.
- [2] G. Allaire and F. Jouve. A level-set method for vibration and multiple loads structural optimization. *Computer Methods in Applied Mechanics and Engineering*, 194(30):3269–3290, 2005.
- [3] G. Allaire, F. Jouve, and A.-M. Toader. Structural optimization using sensitivity analysis and a level-set method. *Journal of Computational Physics*, 194(1):363–393, 2004.
- [4] M. Ansari, A. Khajepour, and E. Esmailzadeh. Application of level set method to optimal vibration control of plate structures. *Journal of Sound and Vibration*, 332(4):687–700, 2013.
- [5] M. Bendsøe. *Methods for optimization of structural topology, shape and material*. Springer Verlag, New York, 1995.
- [6] F. de Gournay. Velocity extension for the level-set method and multiple eigenvalues in shape optimization. *SIAM Journal on Control and Optimization*, 45(1):343–367, 2006.
- [7] A. El-Sabbagh and A. Baz. Topology optimization of unconstrained damping treatments for plates. *Engineering Optimization*, 46(9):1153–1168, 2014.
- [8] Z. Fang and L. Zheng. Topology Optimization for Minimizing the Resonant Response of Plates with Constrained Layer Damping Treatment. *Shock and Vibration*, 2015, Article ID 376854, 2015.
- [9] W. N. Findley and F. A. Davis. *Creep and relaxation of nonlinear viscoelastic materials*. Courier Corporation, 2013.
- [10] F. Hecht. New development in Freefem++. *Journal of Numerical Mathematics*, 20(3-4):251–265, 2012.
- [11] A. Henrot and M. Pierre. *Variation et optimisation de formes: une analyse géométrique*, volume 48. Springer Science & Business Media, 2006.
- [12] K. A. James and H. Waisman. Topology optimization of viscoelastic structures using a time-dependent adjoint method. *Computer Methods in Applied Mechanics and Engineering*, 285:166–187, 2015.
- [13] D. I. Jones. *Handbook of viscoelastic vibration damping*. John Wiley & Sons, 2001.
- [14] F. Jouve. Xd3d. <http://www.cmap.polytechnique.fr/~jouve/xd3d/#Contact>.
- [15] T. Kato. *Perturbation theory for linear operators*, volume 132. Springer Science & Business Media, 2013.
- [16] S. Y. Kim. *Topology design optimization for vibration reduction: reducible design variable method*. PhD thesis, Queen’s University, 2011.
- [17] S. Y. Kim, C. K. Mechefske, and I. Y. Kim. Optimal damping layout in a shell structure using topology optimization. *Journal of Sound and Vibration*, 332(12):2873–2883, 2013.
- [18] Z. Ling, X. Ronglu, W. Yi, and A. El-Sabbagh. Topology optimization of constrained layer damping on plates using Method of Moving Asymptote (MMA) approach. *Shock and Vibration*, 18(1-2):221–244, 2011.
- [19] S. Osher and J. A. Sethian. Fronts propagating with curvature-dependent speed: algorithms based on Hamilton-Jacobi formulations. *Journal of Computational Physics*, 79(1):12–49, 1988.
- [20] G. Parthasarathy, C. Reddy, and N. Ganesan. Partial coverage of rectangular plates by unconstrained layer damping treatments. *Journal of Sound and Vibration*, 102(2):203–216, 1985.
- [21] K. Schreiber. *Nonlinear eigenvalue problems: Newton-type methods and nonlinear Rayleigh functionals*. PhD thesis, Technische Universität Berlin, 2008.

- [22] J. A. Sethian. *Level set methods and fast marching methods: Evolving interfaces in computational geometry, fluid mechanics, computer vision, and materials science*, volume 3. Cambridge University Press, 1999.
- [23] M. van der Kolk, G. J. van der Veen, J. de Vreugd, and M. Langelaar. Multi-material topology optimization of viscoelastically damped structures using a parametric level set method. *Journal of Vibration and Control*, 2015.
- [24] M. Y. Wang, X. Wang, and D. Guo. A level set method for structural topology optimization. *Computer Methods in Applied Mechanics and Engineering*, 192(1):227–246, 2003.
- [25] C. Xu, M.-Z. Wu, and M. Hamdaoui. Mixed integer multi-objective optimization of composite structures with frequency-dependent interleaved viscoelastic damping layers. *Computers & Structures*, 172:81–92, 2016.
- [26] K.-S. Yun and S.-K. Youn. Multi-material topology optimization of viscoelastically damped structures under time-dependent loading. *Finite Elements in Analysis and Design*, 123:9–18, 2017.
- [27] W. Zheng, Y. Lei, S. Li, and Q. Huang. Topology optimization of passive constrained layer damping with partial coverage on plate. *Shock and Vibration*, 20(2):199–211, 2013.